



## Original Article

## Multihazard capacity optimization of an NPP using a multi-objective genetic algorithm and sampling-based PSA

Eujeong Choi<sup>a</sup>, Shinyoung Kwag<sup>b,\*</sup>, Daegi Hahm<sup>a</sup><sup>a</sup> Structural and Seismic Safety Research Division, Korea Atomic Energy Research Institute (KAERI), Daejeon, 34057, Republic of Korea<sup>b</sup> Department of Civil and Environmental Engineering, Hanbat National University, Daejeon, 34158, Republic of Korea

## ARTICLE INFO

## Keywords:

Multihazard  
Multi-objective genetic algorithm  
Probabilistic safety assessment  
Risk informed decision-making  
Capacity optimization

## ABSTRACT

After the Tohoku earthquake and tsunami (Japan, 2011), regulatory efforts to mitigate external hazards have increased both the safety requirements and the total capital cost of nuclear power plants (NPPs). In these circumstances, identifying not only disaster robustness but also cost-effective capacity setting of NPPs has become one of the most important tasks for the nuclear power industry. A few studies have been performed to relocate the seismic capacity of NPPs, yet the effects of multiple hazards have not been accounted for in NPP capacity optimization. The major challenges in extending this problem to the multihazard dimension are (1) the high computational costs for both multihazard risk quantification and system-level optimization and (2) the lack of capital cost databases of NPPs. To resolve these issues, this paper proposes an effective method that identifies the optimal multihazard capacity of NPPs using a multi-objective genetic algorithm and the two-stage direct quantification of fault trees using Monte Carlo simulation method, called the two-stage DQFM. Also, a capacity-based indirect capital cost measure is proposed. Such a proposed method enables NPP to achieve safety and cost-effectiveness against multi-hazard simultaneously within the computationally efficient platform. The proposed multihazard capacity optimization framework is demonstrated and tested with an earthquake–tsunami example.

## 1. Introduction

A nuclear power plant (NPP) is one of the most robust artificial structure systems, ensuring a sufficient safety margin through regular probabilistic safety assessments (PSAs). Often, NPP PSA is performed for single-hazard risk (e.g., seismic PSA), while in reality NPP sites are exposed to the combined effects of various multihazards consisting of more than one hazard. In these circumstances, NPP systems robust against various types of single hazards can remain vulnerable to the effects of multihazards, since securing an NPP system from a single hazard does not necessarily guarantee the multihazard safety of the NPP [1]. For example, the Fukushima Daiichi NPP, which experienced a core damage accident due to an earthquake–tsunami (Japan, 2011) [2], was sufficiently robust from a seismic safety perspective yet prone to the joint effects of strong ground motion and extreme flooding. Therefore, mitigating risk from the multihazard perspective is one of the top priorities of the nuclear power industry. At the same time, not only achieving multihazard safety of NPPs but also reducing the capital cost of NPPs, which is often proportional to the capacity of the structures, systems, and components (SSCs), have become critical issues to produce

cost-competitive commercial nuclear energy.

However, despite the importance of these two issues, cost-informed and system-level multihazard risk-informed design and maintenance planning have not been extensively investigated in the field of nuclear safety engineering. First, the conventional design procedure of an NPP does not account for monetary variables, since preventing core damage is a non-negotiable objective of NPP management authorities. At the same time, NPP safety is typically examined through the individual component-level safety of the SSCs. Such a bottom-up design approach without considering the capital cost results in conservative and expensive design, and does not even necessarily provide the NPP with a system-level multihazard safety margin. Therefore, we aim to identify the optimal relocation of the multihazard capacity of the SSCs of NPPs that minimizes both multihazard risk and capital cost.

To date, in the field of structure and system reliability engineering, various frameworks have been developed to identify the optimal cost- and risk-informed design or maintenance of systems under single-hazard (e.g., earthquake [3–5], hurricane [6], and extreme weather [7]) and multihazard [8,9] conditions. Often, to optimize the retrofitting of a system (e.g., building [10], bridge [11], transportation network [12]),

\* Corresponding author.

E-mail address: [skwag@hanbat.ac.kr](mailto:skwag@hanbat.ac.kr) (S. Kwag).

and power grid [13]), a multi-objective genetic algorithm (MOGA) is combined with system-level functionality, reliability, risk, and life cycle cost analyses.

Especially in the nuclear safety engineering domain, the optimal seismic capacity of the SSCs of NPPs has been studied with consideration of both cost and seismic risk in the work of Kwag and Hahn [14] and Bolisetti et al. [15]. These works identified that the optimal relocation of SSCs can reduce both core damage frequency (CDF) and capital cost compared to the original setting. However, the optimal multihazard capacity of NPPs accounting for both cost and multihazard risk has yet to be investigated. This may be due to the high computational cost for both multihazard risk quantification and the optimization algorithm, as well as the lack of a publicly open capital cost database for NPP SSCs.

Therefore, to address this computational efficiency issue, we propose a framework that combines a MOGA with the two-stage direct quantification of fault trees using Monte Carlo simulation method, or two-stage DQFM [16], which was recently developed by the authors. Also, to resolve the cost data availability issue, we propose a multihazard cost function that uses the hazard capacity of two hazards as an indirect measure. Then to merge the capital costs of two different hazard capacities, the current budget ratio between the two hazard capacities is also adopted. Consequently, such a proposed method enables NPP to achieve safety and cost-effectiveness against multi-hazard simultaneously. Also, combining a MOGA and improved DQFM can secure the efficiency of repetitive risk quantification calculation costs caused by optimization. The proposed methods are demonstrated and tested with a numerical example.

The rest of this paper is organized as follows. Section 2 provides a brief review of multihazard risk quantification methods for NPPs. Next, Section 3 proposes a procedure to identify the optimal multihazard capacity of an NPP. Section 4 demonstrates the proposed framework using the Limerick Generating Station (LGS) NPP as an example. Finally, Section 5 summarizes the paper with concluding remarks.

## 2. Multihazard risk quantification of NPPs

While identifying the optimal risk- and cost-informed multihazard capacity of an NPP, it is essential to evaluate multihazard risk as a type of multi-objective problem. For NPP multihazard risk quantification, several methods have been developed including Boolean [17], original DQFM [18], improved DQFM (I-DQFM) [19], and two-stage DQFM [16]. Among these methods, not a closed-form but a sampling-based algorithm should be adopted to represent partial correlations between the NPP system components. While relatively computationally expensive, sampling-based multihazard risk quantification methods (e.g., I-DQFM, two-stage DQFM) allow to represent not only independent and fully correlated relationships but also partially correlated relationships between the system components. Through a correlation coefficient matrix, the relationships of system components can be accounted for in sampling. Therefore, despite the computational disadvantage of these methods compared to the closed-form methods, sampling-based multihazard risk quantification was preferred for the current work, in which computational efficiency was considered important. In this circumstance, the two-stage DQFM, which was recently developed by the authors, outperforms the others in terms of efficiency and accuracy. Therefore, we adopted two-stage DQFM as the multihazard risk quantification module for the proposed optimization framework. In this section, we briefly summarize the basic idea of the conventional DQFM and two-stage DQFM.

### 2.1. Basic idea of conventional DQFM

The two-stage DQFM uses the conventional DQFM as a base algorithm. This algorithm requires a system model (i.e., fault tree), fragility curve of each component, and hazard curve as inputs, and begins with setting discrete multihazard grids into a uniform interval. For each

hazard point (i.e., a pair of the intensity of hazards 1 and 2), the hazard response  $R$  and the capacity of the components  $C$  are sampled. Both  $R$  and  $C$  are assumed to be log-normal distributions, which can be expressed as follows:

$$R(a) \sim LN(R_m(a), \beta_{Rc}) \quad (1)$$

$$C(a) \sim LN(C_m(a), \beta_{Cc}) \quad (2)$$

where  $LN(\alpha, \beta)$  represents the log-normal distribution with median  $\alpha$  and log-standard deviation  $\beta$ .  $\beta_{Rc}$  and  $\beta_{Cc}$  denote the composite log-standard deviations of  $R$  and  $C$ , respectively. The  $R_m(-)$  and  $C_m(-)$  terms indicate the medians of hazard response and capacity of components, respectively. While randomly generating  $R$  and  $C$  for each hazard, partial correlations between the components can be introduced by the correlation coefficient matrix.

Later, the generated sample set of  $R$  and  $C$  are compared with each other and expressed in binary form (i.e., 0 and 1 represent the survival and failure of the components, respectively). The post-disaster state of a component is considered as survival only when the component survives both hazards. Finally, using the binary condition of each component and the fault tree, the binary state of the system is determined. The final system fragility is estimated as the number of system failures over the total number of samples  $N$  at each multihazard condition [18,19]. With this procedure of the conventional DQFM, the accuracy and variability of the final outcome greatly depend on  $N$ . The computational cost and accuracy of the algorithm increases as  $N$  increases, and vice versa. Such dependency between the accuracy and the computational cost brought the need to develop a more efficient method—the two-stage DQFM.

### 2.2. Two-stage DQFM

The conventional DQFM uses a uniform interval to define the hazard conditions and utilizes a large number of samplings ( $N = 10^4$ ) for all hazard points. However, the contribution of each hazard point to the final multihazard risk value varies by the hazard point. If the contribution of a certain multihazard is trivial to the final risk, the system failure estimated by small  $N_1$  and large  $N_2$  can have negligible difference. With this inspiration, the two-stage DQFM [16], an algorithm that generates a relatively small  $N_1$  (e.g.,  $10^2$ ) sample set for the multihazard points that make a minor contribution to the final multihazard risk while generating a large enough  $N_2$  (e.g.,  $10^4$ ) sample set for others, was proposed in a previous work (Fig. 1) [16].

In the first DQFM stage, a system failure probability is determined for all multihazard points with a small  $N_1$ , which can deliver approximate results with relatively large variability. Using the results of the first DQFM stage, the importance of each multihazard point is identified in terms of its contribution to the final risk. The cumulative ratio of both hazard and risk, which are adopted as the criteria for selecting the resampling points, can be expressed as follows:

$$H_c(a) = \sum_{i^*=1}^a dH(i^*) / dpdq \Bigg/ \sum_{i^*=1}^{\max} dH(i^*) / dpdq \quad (3)$$

$$R_c(a) = \sum_{i^*=1}^a Risk(i^*) \Bigg/ \sum_{i^*=1}^{\max} Risk(i^*) \quad (4)$$

where  $H_c$  and  $R_c$  are the cumulative rates of the differential hazard values and risk values, respectively,  $a$  and  $i^*$  are the newly given order achieved through the min-to-max sorting process (e.g.,  $dH(1)$  is the smallest differential hazard value), and  $p$  and  $q$  denote the intensity of hazards 1 and 2, respectively. Specifically, in the previous two-stage DQFM work [16], the H3.5R20 threshold was identified as the most efficient threshold for multihazard risk evaluation. The H3.5R20 threshold skips the group of points that have an  $H_c$  value smaller than  $10^{-3.5}$  or those that have an  $R_c$  value smaller than 20% in the second (i.e.,  $i^* > 10^{-3.5}$ ).

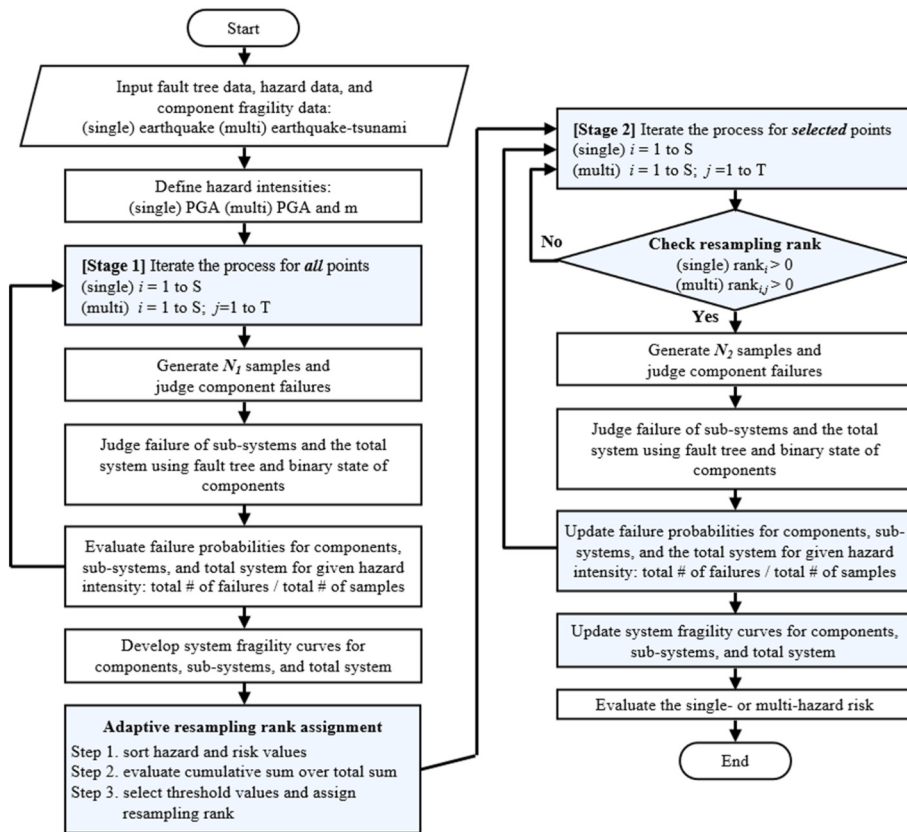


Fig. 1. Flowchart of the two-stage DQFM for multihazard risk quantification (adopted from Ref. [16]).

e., resampling) DQFM stage. With these threshold values, the multi-hazard points that are identified to have a non-negligible contribution to the final risk are sampled again in the second DQFM stage with a large  $N_2$ . Finally, the multihazard risk of the NPP system is determined by a convolution of the hazard curve and the updated fragility curve.

### 3. Multihazard capacity optimization of NPPs based on risk and capital cost

The risk- and cost-informed multihazard capacity optimization framework is proposed in this section. The coupling of the non-dominated sorting genetic algorithm II (NSGA-II [20]) with the two-stage DQFM [16] is described in Section 3.1. Genetic representations for the NPP multihazard capacity, objective functions, and critical zone are described in Sections 3.2 to 3.4., respectively.

#### 3.1. NSGA-II

The NSGA-II is a multi-objective genetic algorithm that is widely applied to the optimization problem of various critical infrastructure systems (CISs) due to its flexibility [12–14] and superior performance out of several MOGAs. In this paper, the authors employ NSGA-II to optimize the multihazard capacity of the SSCs of NPPs with two objectives, i.e., multihazard risk and capital cost. The flowchart of the NSGA-II is illustrated in Fig. 2.

The NSGA-II algorithm begins with generating an initial sample population. With the given population, an offspring sample set is generated using bio-inspired genetic operators (i.e., crossover and random mutation). NSGA-II pursues a balance between elitism and exploration through crossover and random mutation, respectively. After this, the fitness of each sample is determined by the objective functions. Since this work aims to identify the optimal risk- and cost-informed multihazard capacity of SSCs, multihazard risk is evaluated in this

step as one of the objectives using the two-stage DQFM (blue-shaded box in Fig. 2, see also Section 2).

Later, using the objective values of the sample population, a Pareto rank is assigned using fast non-dominated sorting and crowd distance sorting to identify the samples that survive in the next generation. As shown in Fig. 3, the first Pareto rank is assigned to the solutions on the non-dominated surface, after which the solutions except for the first Pareto rank solutions receive the second Pareto rank. Sequentially, other solutions not part of the first and second rank are given the third rank. This procedure is repeated until all sample populations have been Pareto ranked. For sample sets with the same Pareto rank, the distance between the sample sets is used as the second sample selection criteria. Eventually, the sample sets better fitted to the objective functions and more spread out in search space are chosen as parent samples of the following generation.

#### 3.2. Genetic representation

To optimize the multihazard capacity of an NPP using a MOGA, multihazard capacity should be expressed in a genetic representation that is compatible with the algorithm. As illustrated in Fig. 4, we propose a polynomial string that represents multihazard (e.g., seismic and tsunami) capacities. The length of the string can vary by the type of multihazard combination since the number of available risk mitigation options can differ by the characteristics of the hazards.

As an example, a genetic representation of earthquake-tsunami capacity is illustrated in Fig. 4. The seismic capacity can be allocated to each SSC, and therefore the size of the string is required to match the number of SSCs. On the other hand, the tsunami capacity can be assigned for each location (e.g., switchyard, auxiliary building, reactor building), where the SSCs located at the same site or building are considered to have the same tsunami capacity. In Fig. 4,  $n_s$  and  $n_t$  denote the number of SSCs and tsunami-protected locations, respectively, and  $m$

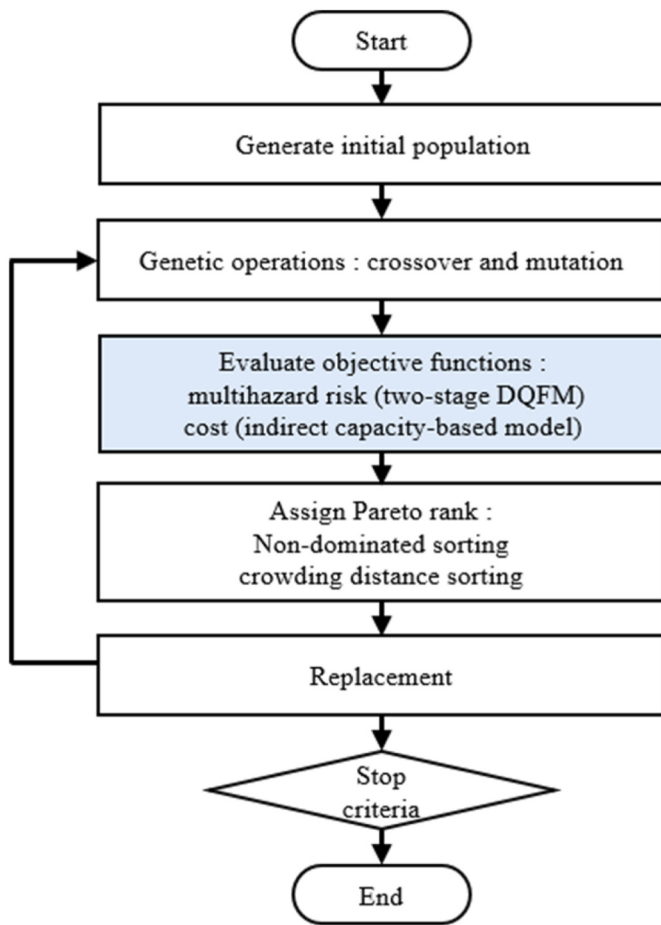


**Fig. 2.** Flowchart of the NSGA-II algorithm.

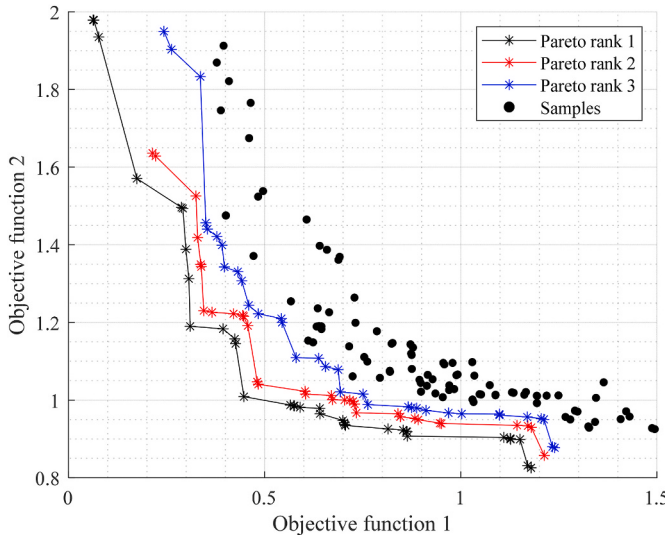


**Fig. 3.** Example of assigning Pareto ranks to sample sets in objective space.

is the population size. The sample population can be expressed in  $(n_s + n_t)$  by  $m$  matrix.

### 3.3. Multi-objective functions

To identify the optimal multihazard capacity of an NPP, two objective functions that generally have a trade-off relationship are selected:

(1) multihazard risk of the NPP, and (2) capital cost. With these objective functions, a group of non-dominated NPP multihazard capacity solutions that minimize both multihazard risk and capital cost of the NPP can be achieved.

#### 3.3.1. Normalized multihazard risk: Core damage frequency (CDF)

The CDF under multihazard conditions is adopted as an objective function to identify the multihazard capacity setting that reduces the multihazard risk. The CDF can be described as:

$$Risk_{multi} = \int_0^{\infty} \cdots \int_0^{\infty} F(p, \dots, q) \frac{dH(p, \dots, q)}{dp \cdots dq} dp \cdots dq \quad (5)$$

where  $p$  and  $q$  denote multihazard intensities, and  $F$  and  $H$  are the system failure probability and multihazard curve, respectively. This CDF risk calculation formula is derived based on the total probability theorem in statistics theory and is a closed-form formulation that is extended to continuous cases according to multihazard characteristics. This formula has been used to calculate multihazard risk problems in structural engineering and nuclear engineering domains (Kameshwar & Padgett, 2014 [21]; Kwag et al., 2019 [19]; Choi et al., 2021 [16]). The multihazard CDF for a given sample population is evaluated by the two-stage DQFM (Section 2.2). In addition, since we pursue to reduce the multihazard CDF of the current NPP, the risk measure is normalized by dividing the CDF of the sample NPP by those of the current NPP as follows:

$$NormalizedRisk_{multi} = Risk_{multi}/Risk_{multi'} \quad (6)$$

where  $Risk_{multi}$  and  $Risk_{multi'}$  denote the CDF of the sample and current NPP, respectively. Therefore, if the CDF of the sample NPP is greater than that of the current NPP, the multihazard risk measure will be greater than unity and vice versa.

#### 3.3.2. Total multihazard capital cost

To identify the optimal multihazard capacity also in terms of capital cost, measuring the capital cost of a given sample is important. If a capital cost database is available and the relationships between the SSC capacities and costs are given, the total capital cost of an NPP can be estimated from the models. For example, in the work of Bolisetti et al. [15], various capital cost functions (e.g., linear, step, square root) were adopted for the seismic fragility of the SSCs. However, this is difficult to apply to most multihazards since the monetary cost data of NPP designs against hazards are not publicly available. Therefore, under the assumption that capital cost is proportional to each hazard capacity [14], an indirect capacity-based cost model, the so-called total multihazard median capacity (TMMC), is proposed in this paper as follows:

$$TMMC = \frac{1}{1 + \alpha} \left( \frac{\sum A_{m1_i}}{\sum A'_{m1_i}} + \alpha \frac{\sum A_{m2_j}}{\sum A'_{m2_j}} \right) \quad (7)$$

where  $A_{m1}$  and  $A_{m2}$  denote the median capacity of the sample set for hazard 1 and 2, respectively, and  $A'_{m}$  is the median capacity of the current NPP. In addition, to combine the cost of two different capacities in one measure, the current budget ratio between the two capacities,  $\alpha$ , is adopted as a weighting factor. If the current cost for the hazard 2 capacity is double that of the hazard 1 capacity, the value of  $\alpha$  is 2. If the estimated cost of the sample is greater than that of the current NPP, the capital cost measure will be greater than unity and vice versa. The reason for combining the cost functions into a single one is that this approach reduces a high-dimensional problem to a low-dimensional problem by using a weighting factor to group two cost functions, allowing for an effective analysis of the results with more restricted constraints in the lower-dimension domain. However, this approach has a limitation in that it cannot continuously check the optimal solution for all weights, so related research is needed in the future. In addition, due to the lack of sufficient cost data for each SSC, uncertainty is not yet

### Sample population matrix

	number of component, $n_s$					number of tsunami-protected locations, $n_t$				
set 1	0.71	2.00	1.60	1.03	0.28	1.22	2.96	16.31	0.07	15.77
set 2	1.02	1.38	1.64	1.30	1.49	1.33	10.62	15.93	10.26	7.83
set 3	1.13	1.11	0.25	1.08	1.11	1.73	9.41	5.09	18.16	8.46
set 4	0.67	1.20	0.78	1.35	0.40	1.18	19.94	5.09	8.67	4.77
⋮	⋮	⋮	⋮	⋮	⋮	⋮	⋮	⋮	⋮	⋮
set $m$	1.57	1.33	1.85	0.80	1.26	0.05	0.26	2.17	9.01	9.36

Fig. 4. Genetic representation of the earthquake–tsunami hazard capacity of an NPP.

considered in this cost model. Through a sufficient cost data archive of NPP SSCs, further realistic cost models that account for uncertainty can be applied. In the scope of this research, we focus on developing a framework for NPP system optimization based on both cost and multi-hazard risk.

#### 3.4. Critical zone

By performing the multi-objective optimization using the functions described in Section 3.3, a group of non-dominated NPP system capacity relocation solutions can be achieved in the cost–risk objective function domain. Yet not all the non-dominated optimal solutions are ideal for the system authorities. Therefore, after achieving the group of non-dominated solutions from the optimization framework, which combines the two-stage DQFM and NSGA-II, the authors only investigate the solutions within a critical zone [12] (Fig. 5).

For the proposed multi-objective functions (Eqs. (6) and (7)), the critical zone is the area that has both normalized risk and cost function values under 1. Cases with either cost or risk value larger than that of the current NPP setting are not considered as alternatives. Therefore, while checking the convergence of the Pareto curve of numerical examples, a

modified area under curve (AUC) [22] is investigated as a measure of the convergence of the results.

## 4. Numerical examples

### 4.1. Problem setting

To demonstrate the proposed framework and to investigate the effect of the weighting factor value (i.e., the ratio between seismic and tsunami capacity cost  $\alpha$ ) and the upper limit of multihazard capacity, an NPP exposed to an earthquake–tsunami multihazard was investigated. The earthquake–tsunami hazard information was taken from a report by the Korea Atomic Energy Research Institute (KAERI) [23] (Fig. 6), and the LGS NPP was considered as an example. The system model and seismic and tsunami capacity of the current NPP setting were adopted from the work of Ellingwood [24] and Kwag et al. [19]. The core meltdown (CM) model is described in Eqs. (8) and (9), which are expanded into Eqs. (10) and (11), and multihazard seismic and tsunami fragility data are summarized in Tables 1 and 2, respectively. The design variable setting for MOGA related to such fragility data is represented in Fig. 7.

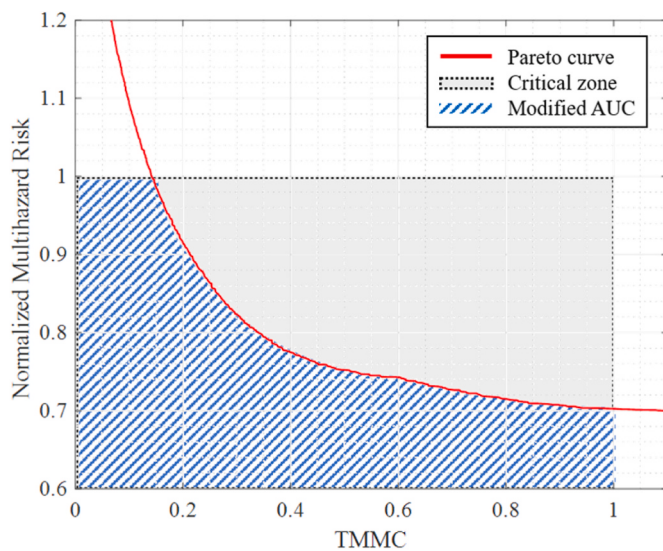


Fig. 5. Conceptual illustration of the critical zone and modified AUC.

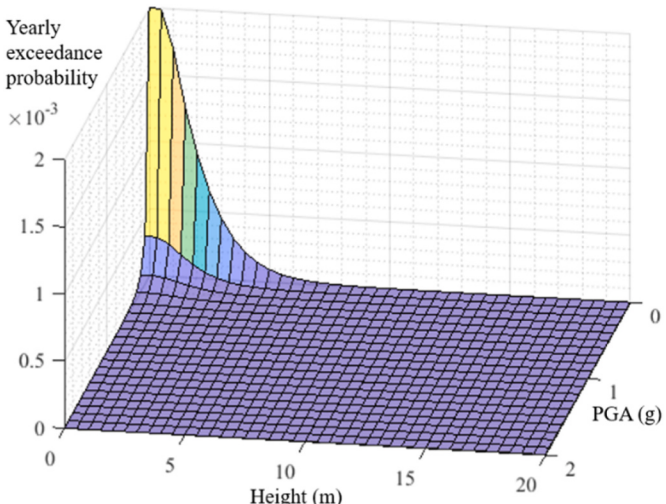


Fig. 6. Earthquake–tsunami hazard information for the numerical example (adopted from Refs. [19,23]).

**Table 1**

Seismic fragility and random failure probability information of LGS NPP components (adapted from Ref. [19]).

Component		$R_{ms}$ ( $A_{ms}$ )	$\beta_{Rcs}$	$B_{Ccs}$	Mean failure rate (per yr)
$S_1$	Offsite power	0.20g	0.226	0.226	–
$S_2$	Condensate storage tank	0.24g	0.273	0.273	–
$S_3$	Reactor internals	0.67g	0.300	0.300	–
$S_4$	Reactor enclosure structure	1.05g	0.282	0.282	–
$S_6$	Reactor pressure vessel	1.25g	0.252	0.252	–
$S_{10}$	Standby liquid control system tank	1.33g	0.233	0.233	–
$S_{11}$	440-V bus/steam generator breakers	1.46g	0.411	0.411	–
$S_{12}$	440-V bus transformer breaker	1.49g	0.397	0.397	–
$S_{13}$	125/250-V DC bus	1.49g	0.397	0.397	–
$S_{14}$	4-kV bus/steam generator	1.49g	0.397	0.397	–
$S_{15}$	Diesel generator circuit	1.56g	0.368	0.368	–
$S_{16}$	Diesel generator heat and vent	1.55g	0.363	0.363	–
$S_{17}$	Residual heat removal system heat exchangers	1.09g	0.330	0.330	–
$DG_R$	DGR – diesel generator common mode	–	–	–	0.00125
$W_R$	WR – containment heat removal	–	–	–	0.00026
$C_R$	CR – scram system mechanical failure	–	–	–	1.00E-05
$SLC_R$	SLCR – standby liquid control	–	–	–	0.01

**Table 2**

Tsunami fragility of LGS NPP components (adapted from Ref. [19]).

Component	$R_{mt}$ ( $A_{mt}$ )	$\beta_{Rct}$	$B_{Cct}$
$S_1$	Offsite power	10 m	0.354
$S_2$	Condensate storage tank	10 m	0.212
$S_{11}$	440-V bus/SG breakers	11 m	0.212
$S_{12}$	440-V bus transformer breaker	11 m	0.212
$S_{13}$	125/250-V DC bus	11 m	0.212
$S_{14}$	4-kV bus/SG	11 m	0.212
$S_{15}$	Diesel generator circuit	11 m	0.212
$S_{17}$	RHR heat exchangers	10 m	0.212

$$A = S_{11} \cup S_{12} \cup S_{13} \cup S_{14} \cup S_{15} \cup S_{16} \cup DG_R \quad (8)$$

$$CM = S_4 \cup S_6 \cup S_1 \cap [A \cup (S_3 \cup C_R) \cap (S_{10} \cup SLC_R) \cap (S_{17} \cup W_R)] \quad (9)$$

$$A = (S_{11s} \cup S_{11t}) \cup (S_{12s} \cup S_{12t}) \cup (S_{13s} \cup S_{13t}) \cup (S_{14s} \cup S_{14t}) \cup (S_{15s} \cup S_{15t}) \cup (S_{16s} \cup S_{16t}) \cup DG_R \quad (10)$$

$$CM = (S_{4s} \cup S_{4t}) \cup (S_{6s} \cup S_{6t}) \cup (S_{1s} \cup S_{1t}) \cup \{A \cup [(S_{3s} \cup S_{3t}) \cap C_R] \cap [(S_{10s} \cup S_{10t}) \cup SLC_R] \cup [(S_{17s} \cup S_{17t}) \cup W_R]\} \quad (11)$$

As summarized in Table 1, some of the system components are likely to have correlated multihazard response and capacity due to their spatial proximity. Therefore, components  $S_{11}$ ,  $S_{12}$ ,  $S_{13}$ , and  $S_{14}$  located in the same reactor building and components  $S_{15}$  and  $S_{16}$  located in the same diesel generator building were assumed to be partially correlated ( $\rho_s = \rho_t = 0.7$ ). A few previous studies have investigated the effects of the correlation coefficient in constructing a multihazard surface (Kwag et al., 2019 [19]; Choi et al., 2021 [16]). The current paper, however, focuses on developing a framework that simultaneously minimizes the SSC capacity cost and risk of NPPs in case of multiple hazards, and thus additional analyses of the optimal solution according to changes in correlation were not considered.

In addition, the current cost ratio between the seismic and tsunami capacity budget  $\alpha$  and the capacity limits for seismic and tsunami capacity should also be selected to perform the optimization. A parametric study on  $\alpha$  was performed with seven values ( $\alpha = 0, 0.25, 0.5, 1, 2, 4$ , and infinity), and its effect on the final Pareto solutions was compared with each other. In addition, under the same  $\alpha$  condition, the effects of six different constraint conditions were also extensively investigated (i.e.,

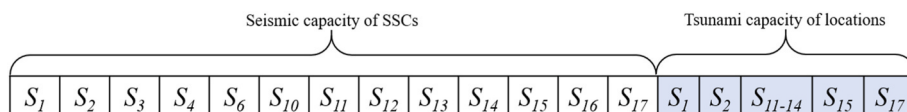
3g, 20 m; 4g, 20 m; 3g, 30 m; 4g, 30 m; 4g, 40 m; 4g, 50 m).

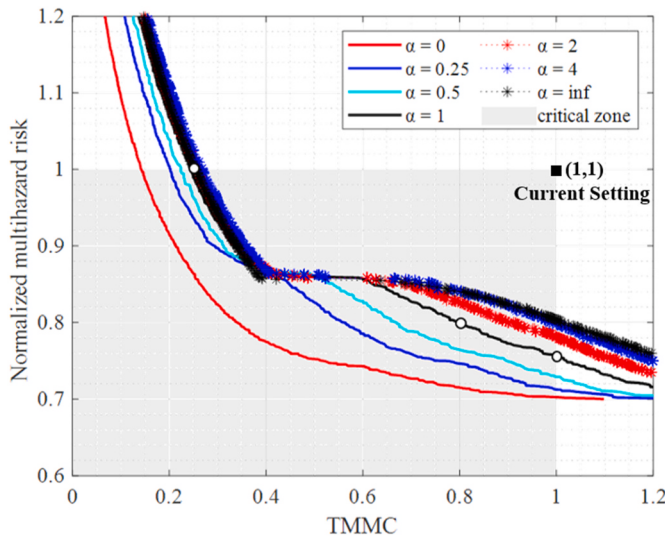
Besides the multihazard budget ratio  $\alpha$  and capacity constraints, various parameters should be selected to perform the proposed method. First, while performing the two-stage DQFM, the seismic intensity (peak ground acceleration PGA, g) and tsunami intensity (inundation depth, m) were uniformly divided into 21 and 41 points, respectively. Also, the H3.5R20 threshold [16] and  $10^2$  and  $10^4$  numbers of samples were used for the first and second stage of the two-stage DQFM, respectively (see Section 2.2). The effectiveness of the two-stage DQFM for the multi-hazard risk evaluation under this parameter setting is also briefly discussed by comparing results with the original DQFM and I-DQFM. Second, for the NSGA-II, a population size of 100, mutation ratio of 1/18 [25], and number of total generations of 1200 were conservatively determined based on several test runs. To check the convergence of the results, a modified AUC (see Fig. 5) was also evaluated over the generations. The numerical investigations were conducted with MATLAB code using a personal computer with a Windows 10 (64 bit) operating system equipped with an Intel(R) Core(TM) i7-9700K CPU @ 3.6 GHz and 16 GB RAM.

## 4.2. Results and discussion

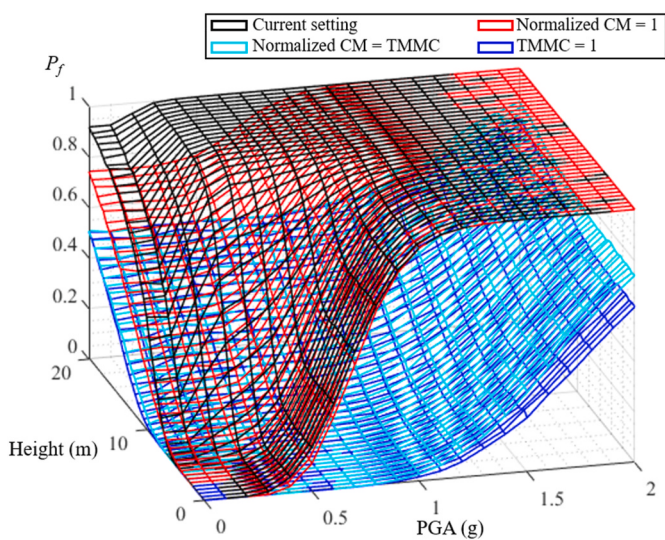
### 4.2.1. Multihazard capacity relocation results for default setting

Fig. 8 shows the Pareto solutions of multihazard capacity relocation of the NPP with seven different earthquake and tsunami capacity budget ratios  $\alpha$  of the current NPP setting (■ symbol) and the critical zone (shaded area). Before investigating the results of the parametric studies, optimal system curves of the NPP and the detailed distribution of the multihazard capacity of each SSC were investigated for the default setting (i.e.,  $\alpha = 1$ ; seismic and tsunami capacity range from 0g to 3g and from 0 m to 20 m, respectively, black line in Fig. 8). The upper limits 3g and 20 m were selected to provide sufficient search space for the algorithm and not to limit the potential optimal solutions by selecting narrow boundaries. It can be noticed in the Pareto curves that normalized multihazard risk and TMMC have a trade-off relationship. Yet in between the TMMC values of 0.4–0.6, there is a region that increases the cost but does not decrease the risk. This is due to the given multihazard upper limit (i.e., 3g and 20 m), which is further discussed in Section 4.2.3 through the parametric study on constraints setting.

**Fig. 7.** Genetic representation of the numerical example.



**Fig. 8.** Pareto solutions of multihazard capacity relocation of the NPP with various  $\alpha$ .



**Fig. 9.** Comparison of the optimal system fragility curves with the current NPP setting (“o” marks in Fig. 8).

Each point constructing the Pareto curve indicates certain non-dominated optimal solutions. Fig. 9 shows the multihazard fragility of the NPP at the system level. In this figure, some of the non-dominated optimal solutions (“o” marks in Fig. 8) are compared with the original NPP conditions. For instance, the red curve indicates a system fragility curve that maintains the current multihazard risk value with only 24.5% of the current NPP cost. While the two-system failure probability (i.e., the black and red curves in Fig. 9) has a negligible difference in most hazard conditions, the red curve shows lower system failure probability at relatively low PGA and high tsunami height conditions, which have a relatively small hazard occurrence probability. On the other hand, the cyan curve indicates a system fragility curve that reduces 20% of both current NPP cost and CM risk, while the blue curve indicates a system fragility curve that maintains the current NPP cost and reduces 24.2% of the current NPP CM risk. In these two cases, the overall system failure probability is smaller than the current NPP setting in most given multihazard conditions.

The detailed seismic and tsunami capacity distribution of each SSC for the TMMC are illustrated in Figs. 10 and 11. In Fig. 10, increases in

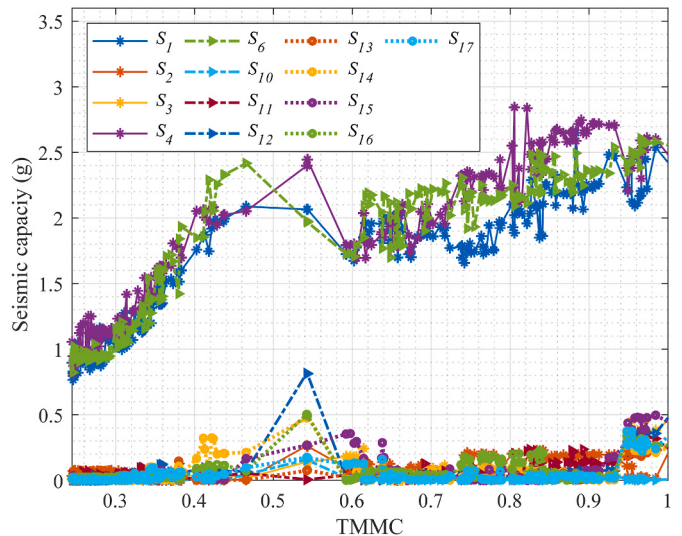


**Fig. 10.** Distribution of the optimal seismic capacities of SSCs for the TMMC.

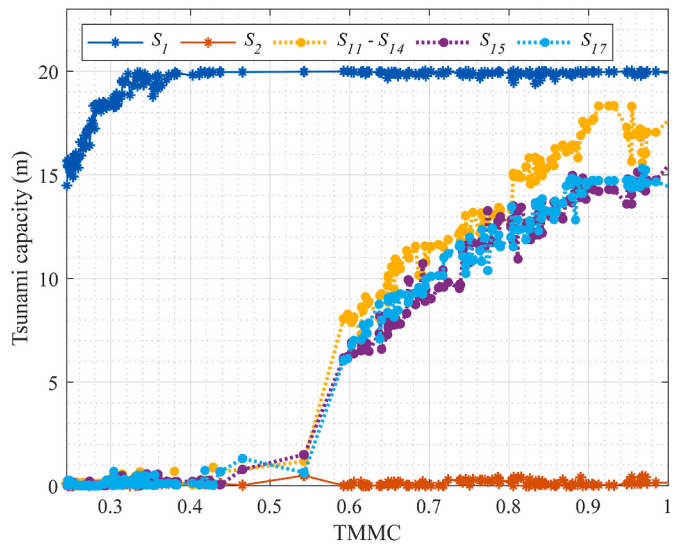


**Fig. 11.** Distribution of the optimal tsunami capacities of NPP locations for the TMMC.

the seismic capacities of  $S_1$ ,  $S_4$ , and  $S_6$  are notable, while other SSCs show little change as the TMMC increases. This may be due to the system model (see Eq. (6)) of CM that has a union relationship with  $S_1$ ,  $S_4$ , and  $S_6$  and intersect relationship with the other SSCs. In Fig. 11, the tsunami capacity of NPP SSCs reaches the upper bound (20 m) at a relatively small TMMC, and other locations  $S_{11}-S_{14}$ ,  $S_{15}$ , and  $S_{17}$  gradually increase where TMMC is greater than 0.6. These indicate that the available budget is first invested in the seismic capacity of  $S_1$ ,  $S_4$ , and  $S_6$  and in the tsunami capacity of  $S_1$  when the multihazard budget is limited. It is interesting that  $S_1$  (Offsite power) is assigned a large capacity for both hazards, while its current seismic and tsunami capacity are the smallest among the SSCs. On the other hand,  $S_2$  (Condensate storage tank), which also has a relatively small capacity in the current NPP setting, was nearly assigned a capacity over all TMMC since it is neglected in the CM model. These results show that the proposed framework identifies the optimal capacity of NPP SSCs with given conditions.

Relocating the optimal capacity for each SSC on a given budget can be challenging as the system model becomes more complex, the system size increases, the system components reflect correlation, and the number of hazards increases. As illustrated in this section, the proposed

method successfully identifies the group of non-dominated solutions with consideration of cost and multihazard risk. Therefore, by supplementing experts' engineering expertise, the proposed method can provide useful insight to management authorities who aim to reduce both multihazard risk and cost of current NPPs.

#### 4.2.2. Parametric study on multihazard budget ratio

In this section, the results of the parametric study on the multihazard budget ratio  $\alpha$  are discussed. It is illustrated in Fig. 8 that further optimal Pareto sample sets, which have smaller values in both objective functions, were delivered as the  $\alpha$  value decreases. These results indicate that the NPP systems of this numerical example have greater potential to reduce both cost and multihazard risk when seismic capacity requires less monetary expense than that of tsunami capacity in the current NPP setting and vice versa.

For example, with multihazard capacity optimization, only 14% and 27% of the current cost is required to maintain the current multihazard risk of the NPP system when  $\alpha$  is 0 and 4, respectively. On the other hand, to maintain the current multihazard capacity cost of the NPP system, only 70% and 80% of the current multihazard risk is expected through multihazard capacity optimization with an  $\alpha$  value of 0 and infinity, respectively. Although  $\alpha$  is unknown for the given example,

these parametric study results on  $\alpha$  indicate that relocation of the seismic and tsunami capacity of NPP SSCs can greatly reduce both cost and multihazard risk, and the results also provide the ranges of potential improvements for NPP systems. Through the proposed framework and objective functions, the management authorities collecting sufficient information to estimate accurate values of  $\alpha$  are expected to deliver more exact optimal multihazard capacity relocation solutions.

In addition, detailed relocation results of NPP SSCs under two extreme  $\alpha$  conditions (i.e., 0 and infinity) are investigated in Fig. 12. Fig. 12 (a,b), (c,d), and (e,f) illustrate the seismic and tsunami capacity of NPP SSCs when the CM is identical to the current NPP, when the normalized CM value and TMMC are equal, and when the TMMC is 1, respectively. When multihazard risk is equal to the current setting and cost is minimized as in Fig. 12 (a,b), it is notable that most of the budget is spent on increasing the tsunami capacity of SSCs up to near upper limits when  $\alpha$  is 0, while little is assigned to the tsunami capacity of SSCs when  $\alpha$  is infinite. This indicates that the proposed algorithm successfully relocates the SSC capacities by minimizing both multihazard risk and cost by prioritizing the cost-efficient hazard capacity.

Similarly, detailed relocation results of NPP SSCs under conditions with five  $\alpha$  values (i.e., 0.25, 0.5, 1, 2, and 4) are also investigated in Fig. 13. When multihazard risk is equal to the current setting and cost is

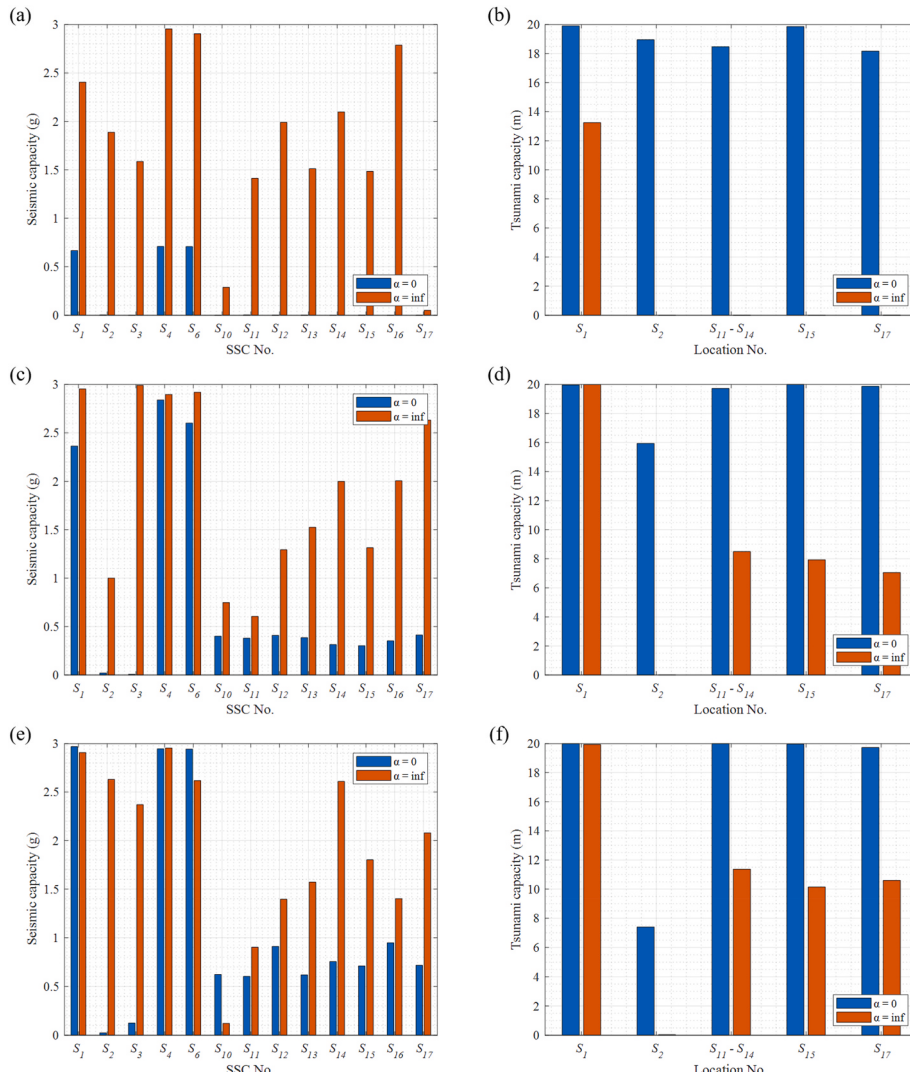


**Fig. 12.** Optimal multihazard capacity solution for all SSCs and NPP locations with various  $\alpha$  (0 and infinity). (a) Seismic capacity of SSCs and (b) tsunami capacity of NPP locations when normalized CM = 1. (c) Seismic capacity of SSCs and (d) tsunami capacity of NPP locations when normalized CM = TMMC. (e) Seismic capacity of SSCs and (f) tsunami capacity of NPP locations when TMMC = 1.

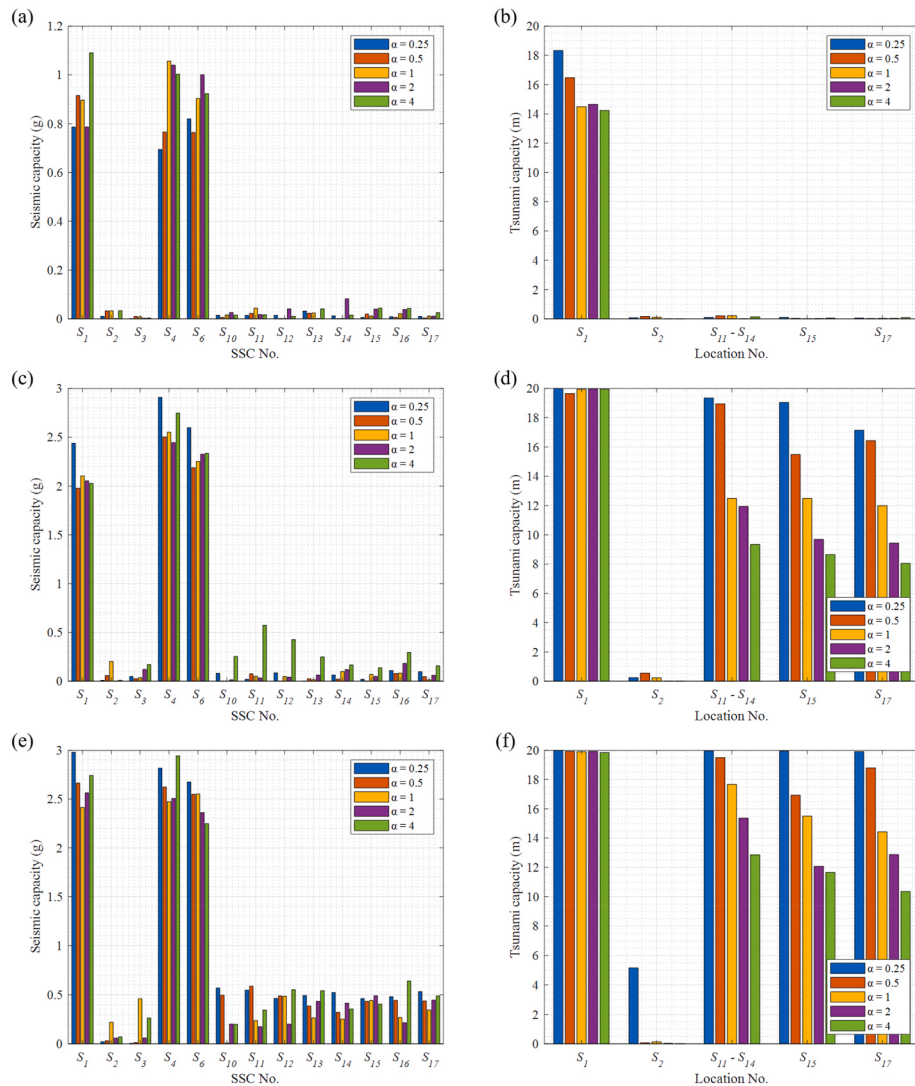


**Fig. 13.** Optimal multihazard capacity solution for all SSCs and NPP locations with various  $\alpha$  (0.25, 0.5, 1, 2, and 4). (a) Seismic capacity of SSCs and (b) tsunami capacity of NPP locations when normalized CM = 1. (c) Seismic capacity of SSCs and (d) tsunami capacity of NPP locations when normalized CM = TMMC. (e) Seismic capacity of SSCs and (f) tsunami capacity of NPP locations when TMMC = 1.

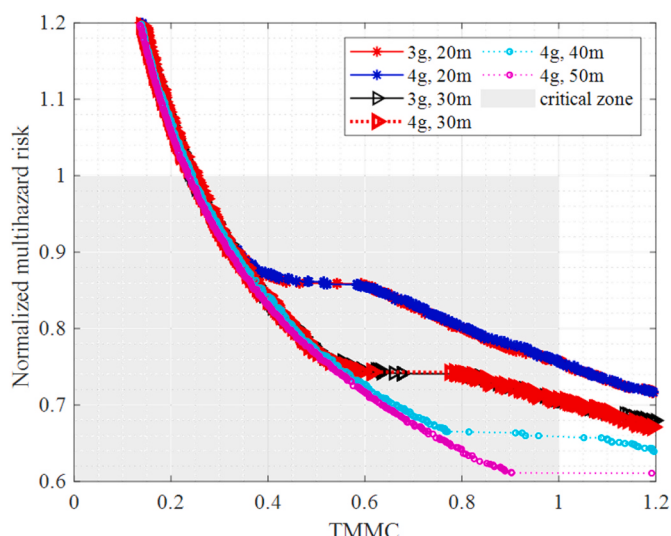


**Fig. 14.** Pareto solutions of multihazard capacity relocation of the NPP with various upper limit constraints.

minimized as in Fig. 13 (a,b), generally, greater seismic capacity is assigned when  $\alpha$  is greater and vice versa. Again, the budget is efficiently spent on increasing the hazard capacity in a cost-effective manner.

#### 4.2.3. Parametric study on multihazard capacity constraints

Besides the multihazard budget ratio, constraints of sample sets also affect the distribution of the Pareto surface. Fig. 14 shows the results of the parametric study on multihazard capacity upper limits. A total of 6 different multihazard capacity constraints were investigated: 3g, 20 m; 4g, 20 m; 3g, 30 m; 4g, 30 m; 4g, 40 m; 4g, 50 m. It is illustrated in Fig. 14 that the final Pareto curves can vary by the multihazard capacity upper limit constraints. In general, Pareto curves with higher upper limit values dominate the curves with smaller upper limit values. However, when the upper limit reaches a sufficient value, further increase of the upper limit does not necessarily deliver a better Pareto curve.

For instance, the Pareto curves in the 3g and 20 m condition (red line in Fig. 14) and 4g and 20 m condition (blue line) have a negligible difference. Similarly, the Pareto curves in the 3g and 30 m condition (black line) and 4g and 30 m condition (red dotted line) show little difference in the critical zone. These results indicate that the optimal seismic capacity of the NPP SSCs does not exceed the 3g upper limit in the given example. On the other hand, an increase of the tsunami upper bound from 20 m to

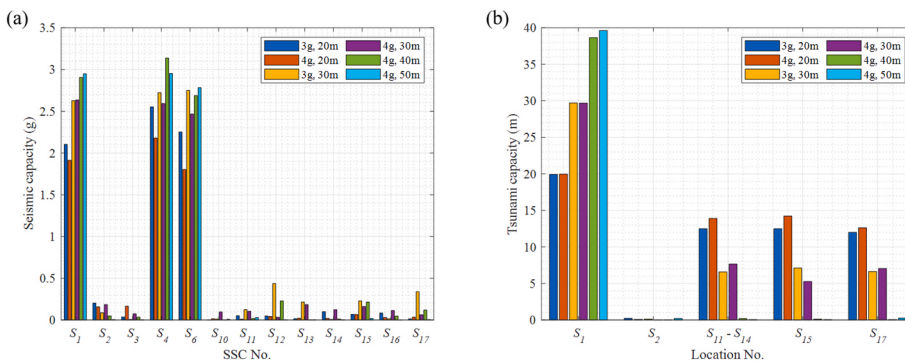


**Fig. 15.** Optimal multihazard capacity solution for all SSCs and NPP locations with various upper limit constraints: (a) seismic capacity of the SSCs and (b) tsunami capacity of NPP locations.

50 m gradually pushes the boundary of the Pareto surface to further optimal objective space.

Detailed relocations of the multihazard capacity of the SSCs, which have a normalized CM value equal to TMMC, are plotted in Fig. 15. It is notable in Fig. 15 (a,b) that the seismic capacity rarely exceeds 3g, while the tsunami capacity of S<sub>1</sub> increases as the upper limit increases.

The parametric study in this section explored potential distributions of the SSCs with various upper limit constraints and found that upper limits under approximately 3g for seismic capacity and approximately 50 m for tsunami capacity can restrict the potential reduction of multihazard risk and cost. However, such sufficient upper limits for seismic and tsunami capacity may be infeasible in practice. Therefore, it is expected that NPP management authorities can identify the optimal SSC multihazard capacities within a feasible solution space using the proposed method to ultimately select feasible upper limits of the SSCs in both hazard capacities.

#### 4.2.4. Verification of the results: computational efficiency and convergence

First, to verify the effectiveness and robustness of the two-stage DQFM compared to other multihazard risk evaluation algorithms, the mean and standard deviation of the CM risk value under the original NPP setting (Tables 1 and 2) were evaluated using three methods, namely original DQFM, I-DQFM, and two-stage DQFM. To minimize the effect of the randomness inherent in the sampling-based approaches, each algorithm was run 50 times; the results are compared in Table 3. As shown in Table 3, the three methods show little difference in the mean value but differ in standard deviation, total computation time, and average number of samples. The conventional DQFM required higher computational cost and more samples than the others. The I-DQFM, on the other hand, required the least computational cost and lowest number of samples among the three methods. However, in terms of performance stability, the two-stage DQFM outperformed the others with smaller standard deviation. For this reason, the authors used the two-stage DQFM even though it requires a 11% higher computational cost than I-DQFM. Compared to the computational demands of the conventional DQFM, the two-stage DQFM requires only 27% of the computational time. This reduction in computational cost enables noteworthy time

**Table 3**  
Results of 50 sets of multihazard CM risk by three different methods.

System Failure Scenario	DQFM		I-DQFM		Two-stage DQFM	
	$\mu$	$\sigma$	$\mu$	$\sigma$	$\mu$	$\sigma$
CM	8.20E-06	4.99E-08	8.19E-06	1.09E-07	8.21E-06	4.95E-08
Total computation time	311.3 s		78.3 s		87.3 s	
Average number of samplings	21*41*4*10 <sup>4</sup>		4*10 <sup>4</sup>		184*4*1*10 <sup>4</sup>	

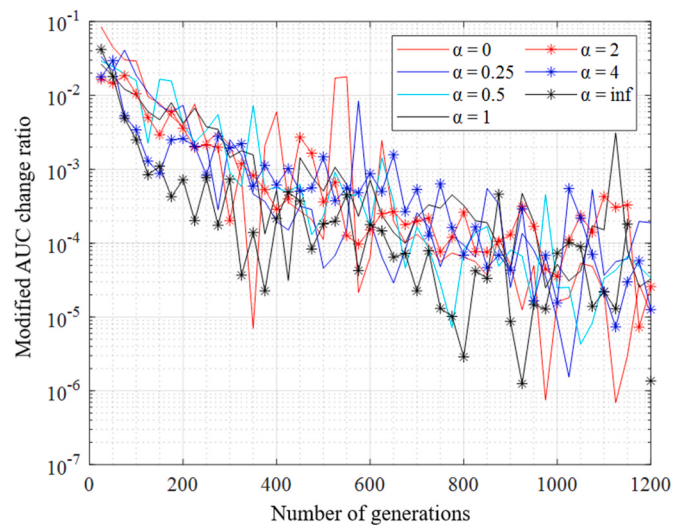


**Fig. 16.** Modified AUC change ratio of the results with various  $\alpha$ .

savings in achieving a set of optimal NPP settings.

In addition, the convergence of the results of NSGA-II was investigated through the modified area under the Pareto curve (defined in Section 3.4 and Fig. 5). It can be noticed in Fig. 16 that Pareto curves with various  $\alpha$  conditions converge with the selected stopping criteria (i.e., 1200th generation), having a change ratio of approximately less than 0.01%.

Since an NPP multihazard event itself is extremely rare in practice, validation of the results in practice is infeasible. To improve the applicability of the results in practice, further realistic cost models and more practical search boundaries should be explored in future research.

#### 4.2.5. Limitations and future research work

Using the proposed method, the optimal multihazard capacity relocation of NPP SSCs was successfully identified with consideration of both cost and multihazard risk. However, several limitations remain and signal the need for future research. First, the proposed objective function for cost is based on the assumption that multihazard cost has a linear relationship with multihazard capacity. However, multihazard capacity is not necessarily linear, and the capacity-cost model can vary by the SSCs. Therefore, an improved objective function for multihazard cost should be developed by further understanding and data of the costs of the SSCs. Second, a single value was assigned as the upper limit of the seismic capacity of all SSCs, and also for the tsunami capacity. Yet different upper limits can be assigned for each SSC based on their characteristics. Although such a setting was not investigated in this paper, the flexibility of the proposed algorithm allows for detailed upper

limit settings for all SSCs. Future research that accounts for both improved capacity-cost models and multihazard capacity limits is expected to deliver more realistic SSC capacity optimization results through the proposed method.

Otherwise, a high computational cost is also one of the limitations of this work. To reach convergence, approximately 2.5 days were required for each run of the proposed method. To date, the two-stage DQFM delivers the best performance among the sampling-based multihazard risk quantification algorithms, while NSGA-II is also known for its superior performance among several MOGAs. However, the combination of these two sampling-based algorithms inherently requires a computational cost that proportionally increases to the square of the problem size. Therefore, further improvement of both the multihazard risk quantification algorithm and multi-objective genetic algorithm is required to facilitate the practical use of the proposed method for large-sized-system problems. Combining a group of improved DQFM-based algorithms [16,26,27] might be one way to tackle this challenge in the future.

## 5. Summary and conclusions

In this study, a multihazard capacity optimization framework that combines NSGA-II and the two-stage DQFM was proposed for NPP SSCs. To perform system-level risk- and cost-informed optimization, genetic representation of the multihazard capacity of NPP SSCs and an indirect cost measure were also proposed. Adaptation of two-stage DQFM for quantification of risk during system optimization using NSGA-II, greatly improves the computational efficiency when compared to the conventional DQFM. Through numerical examples, it was confirmed that the proposed framework and objective functions can successfully identify the optimal SSC multihazard capacity settings that can minimize both risk and cost.

The authors believe that the proposed method can provide useful insight to NPP management authorities by demonstrating a group of optimal system settings. Eventually, the authors expect that the proposed method can not only contribute to system-level multihazard design and protection for NPPs in practice but also increase the cost efficiency of nuclear power production.

## Declaration of competing interest

The authors declare that they have no known competing financial interests or personal relationships that could have appeared to influence the work reported in this paper.

## Acknowledgement

This research was supported by a National Research Foundation of Korea (NRF) grant funded by the Korean government (Ministry of Science and ICT) (No. RS-2022-00154571).

## References

- [1] E. Choi, J. Ha, D. Hahm, M. Kim, A review of multihazard risk assessment: progress, potential, and challenges in the application to nuclear power plants, *Int. J. Disaster Risk Reduc.* 53 (2020), 101933.
- [2] J.E. Yang, Fukushima Dai-Ichi accident: lessons learned and future actions from the risk perspectives, *Nucl. Eng. Technol.* 46 (1) (2014) 27–38.
- [3] B. Zhu, D.M. Frangopol, Risk-based approach for optimum maintenance of bridges under traffic and earthquake loads, *J. Struct. Eng.* 139 (3) (2013) 422–434.
- [4] C. Gomez, J.W. Baker, An optimization-based decision support framework for coupled pre-and post-earthquake infrastructure risk management, *Struct. Saf.* 77 (2019) 1–9.
- [5] N. Xu, R.A. Davidson, L.K. Nozick, A. Dodo, The risk-return tradeoff in optimizing regional earthquake mitigation investment, *Structure and Infrastructure Engineering* 3 (2) (2007) 133–146.
- [6] A. Mondoro, D.M. Frangopol, M. Soliman, Optimal risk-based management of coastal bridges vulnerable to hurricanes, *J. Infrastruct. Syst.* 23 (3) (2017), 04016046.
- [7] R. Rocchetta, Y. Li, E. Zio, Risk assessment and risk-cost optimization of distributed power generation systems considering extreme weather conditions, *Reliab. Eng. Syst. Saf.* 136 (2015) 47–61.
- [8] S. Chandrasekaran, S. Banerjee, Retrofit optimization for resilience enhancement of bridges under multihazard scenario, *J. Struct. Eng.* 142 (8) (2016), C4015012.
- [9] A. Nikellis, K. Sett, Multihazard risk assessment and cost-benefit analysis of a bridge-roadway-levee system, *J. Struct. Eng.* 146 (5) (2020), 04020050.
- [10] M. Liu, S.A. Burns, Y.K. Wen, Multiobjective optimization for performance-based seismic design of steel moment frame structures, *Earthq. Eng. Struct. Dynam.* 34 (3) (2005) 289–306.
- [11] S. Kwag, S.Y. Ok, Robust design of seismic isolation system using constrained multi-objective optimization technique, *KSCE J. Civ. Eng.* 17 (5) (2013) 1051–1063.
- [12] E. Choi, J. Song, Development of Multi-Group Non-dominated Sorting Genetic Algorithm for identifying critical post-disaster scenarios of lifeline networks, *Int. J. Disaster Risk Reduc.* 41 (2019), 101299.
- [13] E. Choi, J. Song, Cost-effective retrofits of power grids based on critical cascading failure scenarios identified by multi-group non-dominated sorting genetic algorithm, *Int. J. Disaster Risk Reduc.* 49 (2020), 101640.
- [14] S. Kwag, D. Hahm, Multi-objective-based seismic fragility relocation for a Korean nuclear power plant, *Nat. Hazards* 103 (3) (2020) 3633–3659.
- [15] C. Bolisetti, J. Coleman, W. Hoffman, A. Whittaker, Cost-and risk-based seismic design optimization of nuclear power plant safety systems, *Nucl. Technol.* 207 (11) (2021) 1687–1711.
- [16] E. Choi, S. Kwag, J. Ha, D. Hahm, Development of a two-stage DQFM for efficient single- and multi-hazard risk quantification for nuclear facilities, *Energies* 14 (4) (2021) 1017.
- [17] F.L. Leverenz, H. Kirch, User's Guide for the WAM-BAM Computer Code (No. PB-249624), Science Applications, Inc., Palo Alto, CA., USA, 1976.
- [18] Y. Watanabe, T. Oikawa, K. Muramatsu, Development of the DQFM method to consider the effect of correlation of component failures in seismic PSA of nuclear power plant, *Reliab. Eng. Syst. Saf.* 79 (3) (2003) 265–279.
- [19] S. Kwag, J.G. Ha, M.K. Kim, J.H. Kim, Development of efficient external multi-hazard risk quantification methodology for nuclear facilities, *Energies* 12 (20) (2019) 3925.
- [20] K. Deb, A. Pratap, S. Agarwal, T.A.M.T. Meyarivan, A fast and elitist multiobjective genetic algorithm: nsga-II, *IEEE Trans. Evol. Comput.* 6 (2) (2002) 182–197.
- [21] S. Kameshwar, J.E. Padgett, Multi-hazard risk assessment of highway bridges subjected to earthquake and hurricane hazards, *Eng. Struct.* 78 (2014) 154–166.
- [22] A.P. Bradley, The use of the area under the ROC curve in the evaluation of machine learning algorithms, *Pattern Recogn.* 30 (7) (1997) 1145–1159.
- [23] KAERI, Development of Site Risk Assessment & Management Technology Including Extreme External Events, Korea Atomic Energy Research Institute, Daejeon, South Korea, 2017. KAERI/RR-4225/2016.
- [24] B. Ellingwood, Validation studies of seismic PRAs, *Nucl. Eng. Des.* 123 (1990) 189–196.
- [25] G. Ochoa, Setting the mutation rate: scope and limitations of the 1/L heuristic, in: *Proceedings of the 4th Annual Conference on Genetic and Evolutionary Computation*, Morgan Kaufmann Publishers Inc., 2002.
- [26] S. Kwag, S. Eemb, E. Choi, J.G. Ha, D. Hahm, Toward improvement of sampling-based seismic probabilistic safety assessment method for nuclear facilities using composite distribution and adaptive discretization, *Reliab. Eng. Syst. Saf.* 215 (2021), 107809.
- [27] Kwag, S., Eemb, S., Choi, E., Hahm D. Eemb, S., and Ju, B. On Improving Seismic Risk and Cost for Research Reactor Based on Multi-Objective Optimization Considering Seismic Correlation. (*Under Review*).